# Lipschitz Regularized Interval Estimation for Optimal Power Flow Reachability

Gaoyuan Xu, Peng Zhang
*Department of Electrical and Computer Engineering*
*Stony Brook University*
Stony Brook, NY, USA
{gaoyuan.xu, p.zhang}@stonybrook.edu

***Abstract*—This paper presents a Lipschitz-based method for constructing interval enclosures of optimal power flow (IntervalOPF) solutions under load uncertainty. The proposed approach requires only a single additional OPF evaluation beyond the midpoint solution to estimate the solution enclosure. We establish theoretical foundations for IntervalOPF by analyzing the local Lipschitz continuity of the OPF solution mapping and by showing how a small number of randomized extreme-direction probes can approximate the Lipschitz constant. This leads to a lightweight and theoretically justified interval estimator that readily scales to large systems. Numerical experiments on benchmark OPF test cases demonstrate that IntervalOPF produces reliable enclosures and achieves substantial computational savings compared with exhaustive Monte Carlo samplings, while maintaining high empirical coverage. These results indicate that IntervalOPF provides a practical, accurate, and scalable tool for uncertainty-aware OPF analysis.**

***Index Terms*—Interval analysis, Lipschitz continuity, virtual dynamics, optimal power flow, uncertainty**

## I. Introduction

Volatility from AI data centers and inverter-based resources (IBRs) poses major challenges for optimal power flow (OPF) computation. Consequently, analyzing OPF behavior under uncertainty has become essential for secure and reliable grid operation, enabling accurate dispatch [1], robust security assessment [2], and informed economic decision-making [3].

One promising approach for characterizing system uncertainty is reachability analysis, which seeks to enclose all possible trajectories or steady-state outcomes of a dynamical or algebraic system under disturbances. Reachability offers several safety verification, worst-case performance certification, and robustness assessment across entire uncertainty sets rather than individual scenarios [4]. Recent applications in power systems have successfully applied reachability ideas to microgrid dynamics and networked systems [5]. For examples, we developed neuro-reachability methods for networked microgrids to capture nonlinear transient behaviors under disturbances [6]; explored reachable dynamics under large disturbances [7]; established reachable power flow for steady-state feasibility under uncertainties [8]; and proposed reachable eigenanalysis [9]. These methods highlight the potential of reachability theory to provide rigorous, set-based guarantees in power system analysis, enabling applications such as stability certification, safe operation envelopes, and secure control design.

Despite these advances, extending reachability analysis to OPF remains challenging because the AC power-flow equations are highly nonlinear and nonconvex. In [10], a Lyapunov function was introduced to construct a virtual-dynamics representation of the OPF conditions. However, in the neighborhood of a primal feasibility point, certain slack or dual variables may approach zero or diverge to large magnitudes, making the associated dynamics highly sensitive to stepsize choices. Without a globalization mechanism—such as a line-search or trust-region strategy—an improperly scaled update can easily drive the virtual state outside the stability region [11]. Consequently, existing reachability and verification frameworks for continuous-time optimization cannot be directly applied to the virtual-dynamics formulation of AC-OPF to certify solution bounds under parameter uncertainty. To address this limitation, this paper devises *IntervalOPF*, a sample-efficient Lipschitz-based method that directly bounds the OPF solution map and provides reliable interval estimates for nonconvex AC-OPF problems. Major new contributions of this paper are as follows:

- *Devising a dynamics-free interval method for OPF sensitivity:* We introduce a novel interval construction approach that estimates the variation of OPF solutions under uncertainties without requiring the computationally costly integration of virtual dynamics. The method relies solely on a single OPF solution at the uncertainty midpoint and a single adjoint sample at a randomized extreme-direction, making it extremely efficient and easy to implement for large-scale systems.
- *Lipschitz-guided interval estimation framework.* We establish a theoretical rationale for the proposed interval estimation framework by analyzing the local Lipschitz regularity of the OPF solution mapping. We show that Lipschitz-regularized scaling serve as an effective sampling-based mechanism to construct empirical upper-bound estimates that yield reasonable solution intervals under broad operating conditions.
- *Extensive experiments demonstrating accuracy, scalability, and practicality.* Numerical studies on benchmark OPF test cases verify that IntervalOPF achieves tight interval enclosures with orders-of-magnitude speedup compared to exhaustive sampling methods. The results confirm that IntervalOPF provides a practical and scalable tool for uncertainty-aware OPF analysis in operational settings.

979-8-3315-8138-1

## II. Virtual Dynamic-Based OPF Model

### A. Steady-State OPF Model

The standard AC-OPF in compact form is modeled as:

$$\begin{aligned} \min_{x} \quad & f(x) \\ \text{s.t.} \quad & g(x,p) = 0, \\ & h(x,p) \leq 0. \end{aligned} \tag{1}$$

where

- $x$ denotes the system state, including voltage magnitudes $V$, voltage angles $\theta$, generator active/reactive setpoints $(P_G, Q_G)$.
- $p$ denotes uncertain or varying load/generation parameters (active/reactive power injections $(P_D, Q_D)$).
- $g(x,p) = 0$ are the nonlinear power flow equations.
- $h(x,p) \leq 0$ represents operational inequality constraints including generator limits and voltage limits.

### B. OPF Newton Flow

The optimal solution of problem (1) has a zero measure on all partial derivatives of lagrangian function. In an abstraction:

$$F(q) = \nabla_{x,Z,\lambda,\mu}\mathcal{L}(x,Z,\lambda,\mu) = 0 \tag{2}$$

where $Z$ are slack variables and $\lambda, \mu$ are dual variables. Please refer to section 3.3 of [12] for expanded lagrangian function formulation. Following the idea of solving power flow equations by Newton-Raphson (NR) method in [13], the Newton steps generate a numerical solution to Eq. (2), as follows:

$$q_{k+1} = q_k - \left(F_q(q_k,p)\right)^{-1} F(q_k,p), \tag{3}$$

where $q_k$ denotes the value of $q$ at k$^{\text{th}}$ iterations and $F_q(q_k)$ denotes the partial derivatives of $F(q)$ at $q_k$. $p$ as parameter (such as active load $P_D$) is fixed during iterations. Converting discrete iterations (3) into a discrete-time virtual dynamics, we define the *OPF Newton flow* as follows:

$$q^+(t) = -F_q(q(t),p)^{-1}F(q(t),p) = K(q(t),p), \tag{4}$$

where $t$ plays the role of a virtual iteration time. If equation (4) satisfies for all $p$ in the uncertainty set

$$q^+(t) = 0 \quad \Longleftrightarrow \quad F(q,p) = 0,$$

any equilibrium of the Newton flow corresponds exactly to one solution of the optimality conditions of the OPF problem.

While the virtual dynamics for power flow equations admit a well-defined Jacobian, the Newton flow of the OPF KKT system does not share this property. Step size strategies are commonly used for choosing step size $\alpha_k$ to enforce convergence, e.g., trust-region Newton method in MIPS [14]. Different uncertainty typically require different sequences of step sizes to maintain descent direction and feasibility. As a result, it is impractical to identify a constant step size that simultaneously guarantees convergence and feasibility for all elements of the evolving set at each iteration. This fundamental incompatibility renders set propagation in [15] ill-suited for OPF reachability analysis, motivating the interval approach proposed in Section III-B.

## III. IntervalOPF Algorithm

### A. Interval Arithmetic

Interval arithmetic provides a fundamental framework for propagating bounded uncertainty through nonlinear functions. Given a scalar variable $x$ which is bounded, its interval representation is defined as

$$[x] = [\underline{x}, \overline{x}] = \{\, x \in \mathbb{R} : \underline{x} \leq x \leq \overline{x}, \underline{x} \leq \overline{x} \,\}.$$

For vector-valued variables $x \in \mathbb{R}^n$, the corresponding interval (hyper-rectangle) is defined componentwise.

For a real-valued function $f : \mathbb{R}^n \to \mathbb{R}$, an *interval extension* of $f$ is a mapping

$$F([x]) = [\, \underline{f}, \overline{f} \,]$$

such that

$$f(x) \in F([x]) \quad \text{for all } x \in [x].$$

Interval extensions can be built using four basic operations defined in [16].

### B. Interval OPF Caculation

Let the uncertainty set for the parameters be:

$$p \in [p] = [p_{\mathrm{mid}} - p_{\mathrm{rad}},\ p_{\mathrm{mid}} + p_{\mathrm{rad}}]. \tag{5}$$

There are various sources of uncertainties in OPF [17], including load variations, changes of objective function coefficients, Y matrix or even topology, etc. In this paper, we only consider the uncertainty of $P_D$. Given uncertainty $[p]$, we aim to construct an interval enclosure for OPF solution $[q] = OPF([p])$. Now, we denote the interval enclosure as:

$$[q] = [q_{\mathrm{mid}} - q_{\mathrm{rad}},\ q_{\mathrm{mid}} + q_{\mathrm{rad}}],$$

where $q_{\mathrm{mid}}$ is typically chosen as the $OPF(p_{\mathrm{mid}})$. In [16], growth bound method seeks to find the largest distance away from the center, e.g., $(q_{\mathrm{mid}}, p_{\mathrm{mid}})$ in our context, among a prefixed region by constructing a growth bound function $G(t_0, t_f, [x], [p])$, which requires calculating the upper bound of the infinity measure of Jacobian matrix $\max \mu_\infty(J_x)$. Quasi-Monte Carlo method seeks to equally divide the interval of $x$ and $p$ and apply growth bound function to each subinterval. Essentially, the difference between growth bound method and [15] lies mostly on the set representation of the uncertainty. Growth Bound method only allows intervals while [15] allows zonotope and ellipsoid, etc.

To calculate the Jacobian of $F(q)$ in Eq. (2), we apply taylor expansion to the virtual dynamics (4) at $q = q_{\mathrm{mid}}$ and $p = p_{\mathrm{mid}}$:

$$\dot{q}(t) = A(t)(q(t) - q_{\mathrm{mid}}) + B(t)(p - p_{\mathrm{mid}}) + \varepsilon(t) \tag{6}$$

where:

$$A = \left.\frac{\partial K}{\partial q}\right|_{q_{\mathrm{mid}},p_{\mathrm{mid}}} = -F_q^{-1}\frac{\partial F_q}{\partial q}K - I \tag{7}$$

$$B = \left.\frac{\partial K}{\partial p}\right|_{q_{\mathrm{mid}},p_{\mathrm{mid}}} = -F_q^{-1}\frac{\partial F_q}{\partial q}K - F_q^{-1}\frac{\partial F}{\partial q} \tag{8}$$

979-8-3315-8138-1

**Algorithm 1** INTERVALOPF algorithm

**Result:** $\{(x^m_{\mathrm{mid}}, x^m_{\mathrm{rad}})\}_{m=1}^{M}$
**Initialization:** $[p]$, $\ell$, $M = \prod_{i=1}^{n} \ell^i$;
Divide $[p]$ with $v$ subintervals and get $\{(p^m_{\mathrm{mid}}, p^m_{\mathrm{rad}})\}_{m=1}^{M}$, calculate $\kappa = \frac{\sum_j P_D^j}{\max_j P_D^j}$
**for** $m = 1$ to $M$ **do**
  Solve OPF problem (3) with $P^m_{\mathrm{mid}}$, to get $x^m_{mid}$;
  Select $p^m_{rand}$ with $||p^m_{rand} - p^m_{\mathrm{mid}}|| = p^m_{\mathrm{rad}}$;
  Solve system (3) with $p^m_{rand}$, to get $x^m_{rand}$;
  Apply trajectory bound coefficient $\kappa$ to get $x^m_{\mathrm{rad}}$.
**end for**

and $\varepsilon(t)$ represents the nonlinear terms. Given uncertainty set $[p]$, we can derive the interval matrix $[F_q]$, however, computing an exact or finite inverse interval matrix $[F_q^{-1}]$ is NP-hard [18].

Instead of deriving closed form for the radius, we can estimate the radius using samples and apply sampling-based approach to obtain the final interval. Denote $p^i_{rad} = r^i P^i_D$, $\Delta p^i = \beta^i P^i_D$, then we have $\beta^i \leq r^i$. Assume that the OPF operator has $L_p$-lipschitz continuity, which is defined as

$$||\Delta x^i|| \leq L_p^i ||p||_\infty \tag{9}$$

$$L_p^i = \sup_{0 \leq ||\beta||_\infty \leq r} \left( \frac{||\Delta x||}{||\Delta p||_\infty} \right) \tag{10}$$

where $||\Delta x^i||$ is the $i^{\text{th}}$ component in $\Delta x$. Next, we derive the *trajectory bound* for our algorithm:

$$||\Delta x^i|| \leq L_p^i ||p||_\infty \leq L_p^i ||p||_1 \tag{11}$$

$$= \sup \frac{||\Delta x||_i}{||\Delta p||_\infty} \times \sum_{j \in B} P_D^j ||\beta||_\infty \tag{12}$$

$$= \sup \frac{||\Delta x||_i}{\max_{j \in S} r^j P_D^j} \times \sum_{j \in B} P_D^j ||\beta||_\infty \tag{13}$$

$$\leq \underbrace{\frac{\sum_{j \in B} P_D^j}{\max_{j \in B} P_D^j}}_{\kappa} \times \underbrace{\frac{\max_{j \in B} P_D^j}{\max r^j P_D^j} \left(\sup ||\Delta x||_i ||\beta||_\infty\right)}_{\tilde{r}} \tag{14}$$

where $B$ is the set of all buses. If we select $p^m_{\mathrm{rand}}$ at any corner of the parameter interval, i.e., $||\beta||^i = r^i$, then we can set $|x^m - x^m_{\mathrm{mid}}|$ as a sample estimate for $\tilde{r}$ so that the estimated $\tilde{q}_{\mathrm{rad}}$ is

$$\tilde{q}_{\mathrm{rad}} = \kappa |x^m_{\mathrm{rand}} - x^m_{\mathrm{mid}}| \tag{15}$$

### *C. IntervalOPF Algorithm*

Our proposed algorithm is shown in Algorithm 1. The algorithm reliably estimates the enclosure of all OPF solutions corresponding to the parameter interval $[p]$ by a hyper-rectangles characterized by $(x^m_{\mathrm{mid}}, x^m_{\mathrm{rad}})$ for $m = 1, \ldots, M$.

*1) Initialization:* Given a nominal parameter vector $p_{\mathrm{mid}}$ and an interval radius $p_{\mathrm{rad}} \geq 0$, the uncertain parameter set is initialized by Eq. (5). To increase accuracy, $[p]^i$ is further divided along each component into $\ell^i$ subintervals, $i = 1, \ldots, n_x$,where $n_x$ is the dimension of the OPF state vector. The total number of subintervals is $M = \prod_{i=1}^{n} \ell^i$.
*2) Nominal OPF solution within each subinterval:* For the $m$-th subinterval, OPF problem (1) with parameter $p^m_{\mathrm{mid}}$ is solved. The resulting state is denoted by $x^m_{\mathrm{mid}}$.
*3) Trajectory sampling and radius computation:* To capture the worst-case deviation within the $m$-th subinterval, a boundary parameter sample $p^m_{\mathrm{rand}}$ is selected such that $\|p^m_{\mathrm{rand}} - p^m_{\mathrm{mid}}\| = p^m_{\mathrm{rad}}$. Solving OPF problem (1) with parameter $p^m_{\mathrm{rand}}$, we generate a sample result $x^m_{\mathrm{rand}}$ starting from a prescribed initial point $x^m_{\mathrm{mid}}$. According to Eq. (15), the distance $|x^m_{\mathrm{rand}} - x^m_{\mathrm{mid}}|$ is multiplied by $\kappa$ to construct a componentwise radius $x^m_{\mathrm{rad}}$ such that

$$|x - x^m_{\mathrm{mid}}| \leq x^m_{\mathrm{rad}}$$

holds for all OPF solutions corresponding to parameters $p$ in the $i$-th subinterval. In other words, the hyper-rectangle $[x^i_{\mathrm{mid}} - x^i_{\mathrm{rad}},\, x^i_{\mathrm{mid}} + x^i_{\mathrm{rad}}]$ forms an interval enclosure of the local reachable OPF set.
*4) Overall enclosure:* After repeating Steps 2) – 3) for all $M$ subintervals, the global interval OPF result is obtained as the union of all local boxes. The collection $\{(x^m_{\mathrm{mid}}, x^m_{\mathrm{rad}})\}_{m=1}^{M}$, returned by Algorithm 1, provides a tractable over-approximation of all OPF solutions under the parameter uncertainty $[p]$.

## IV. CASE STUDIES

### *A. Experimental Setup*

All numerical experiments were implemented in MATLAB R2025b using the MATPOWER and MIPS toolboxes. Computations were performed on a workstation equipped with an Intel Core i7 processor (2.50 GHz) and 64 GB of RAM running 64-bit Windows 11. The implementation uses sparse linear algebra and parallel toolbox with 8 cores for $v \geq 2$ to ensure numerical efficiency as well.

The *IntervalOPF* method is first evaluated on the IEEE 39-bus system. The default active-power load uncertainty is set to 10%, i.e., $p^i \in [0.9, 1.1] P^i_D$. We consider uncertainty on the buses with the top $n_{\mathrm{u}}$ active loads, with $n_{\mathrm{u}} = 3$ unless otherwise specified. The exhaustive Monte Carlo method, obtained by uniformly traversing the $P_D$ uncertainty space, has sample complexity $O(d^{n_{\mathrm{u}}})$, where $d$ denotes the number of discretization levels per load dimension (including endpoints). In all experiments, we set $d = 16$, so there are $S = d^{n_{\mathrm{u}}}$ Monte Carlo samples. In contrast, the proposed approach partitions each uncertainty dimension into $v$ subintervals, resulting in a total complexity of $O(\ell^{n_{\mathrm{u}}})$. Our proposed method thereby achieves, depending on the choice of $\ell$, either constant complexity when $\ell = 1$ or a polynomial speedup of $\left(\frac{d}{\ell}\right)^{n_{\mathrm{u}}}$ relative to the exhaustive Monte Carlo baseline.

### *B. Numerical Results of IntervalOPF*

In this subsection, we illustrate the performance of the proposed IntervalOPF framework on a sequence of test cases in 39-bus

979-8-3315-8138-1

TABLE I: Comparison of IntervalOPF and Monte Carlo: Runtime and Coverage Percentage.

| **Case** | $n_{\mathrm{u}}$ | $T_{\mathrm{MC}}$ **(s)** | $\ell$ | $T_{\mathrm{Int}}$ **(s)** | **Pct. (%)** |
|---|---|---|---|---|---|
| Case 9 | 3 | 181 | 4 | 1.59 | 88.26 |
| Case 39 | 2 | 25 | 4 | 0.77 | 89.27 |
| | 3 | 376 | 1 | 0.28 | 64.11 |
| | | | 2 | 0.54 | 90.47 |
| | | | 3 | 1.32 | 93.50 |
| | | | 4 | 2.83 | 93.56 |
| | 4 | 5502 | 4 | 10.57 | 95.38 |
| Case 118 | 3 | 1737 | 4 | 13.68 | 90.04 |
| Case 300 | 3 | 6011 | 4 | 85.98 | 94.50 |

system with increasing uncertainty dimension $n_{\mathrm{u}}$, different interval orders $\ell$, and varying levels of load uncertainty.

**1) Impact of interval order**

We evaluates the impact of the interval order $\ell$ on both runtime and coverage for the 39-bus system, with $\ell = 1, 2, 3, 4$. We define the average coverage percentage as the fraction of Monte Carlo samples whose OPF solutions lie within the constructed interval enclosure, averaged over all state variables. As shown in Figure 1 and Table I, increasing $\ell$ refines the partitioning of each uncertainty dimension and leads to a computational cost that scales approximately as $O(\ell^{n_{\mathrm{u}}})$. At the same time, higher interval orders yield consistently tighter enclosures and improved coverage, with the $\ell = 3$ case already significantly reducing the radius $x_{\mathrm{rad}}$ compared with $\ell = 2$.

We evaluate the impact of the interval order $\ell$ on both runtime and coverage for the 39-bus system, with $\ell = 1, 2, 3, 4$. We define the average coverage percentage as follows. For each Monte Carlo sample $x^s$ with true OPF solution $x^s_{\mathrm{MC}}$, let the coverage percentage $\xi^s$ denote the maximum fraction of dimension of state variables whose entries lie within a single interval enclosure produced by *IntervalOPF*. Formally,

$$\xi^s = \frac{1}{n_x} \max_{m \in \{1,\dots,M\}} \sum_{i=1}^{n_x} \mathbf{1}\left\{ x^s_{\mathrm{MC},i} \in [x^m_{\mathrm{min},i}, x^m_{\mathrm{max},i}] \right\}.$$

The average coverage percentage is then defined as the empirical mean $\frac{1}{S}\sum_{s=1}^{S} \xi^s$ over all $S$ Monte Carlo samples.

As shown in Figure 1 and Table I, increasing $v$ refines the partitioning of each uncertainty dimension and yields a computational cost that scales approximately as $O(\ell^{n_{\mathrm{u}}})$. At the same time, higher interval orders produce consistently tighter enclosures and improved coverage, with the $v = 4$ case already significantly reducing the radius $x_{\mathrm{rad}}$ relative to $v = 1$.

To further quantify the behavior of the coverage percentage, we examine the empirical distribution of the per-sample coverage ratios $\xi^s$ for different interval orders $v$. Figure 2 shows the estimated probability density functions of $\xi^s$ as

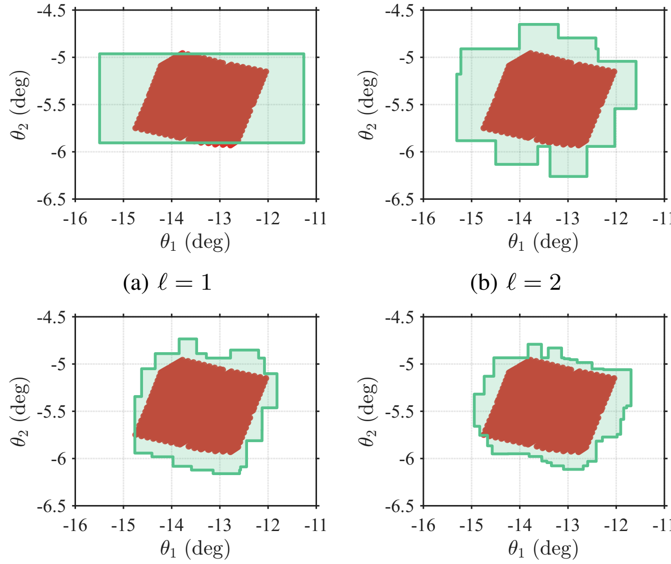


(a) $\ell = 1$ (b) $\ell = 2$ (c) $\ell = 3$ (d) $\ell = 4$

Fig. 1: Comparison across interval orders $\ell = 1, 2, 3, 4$.

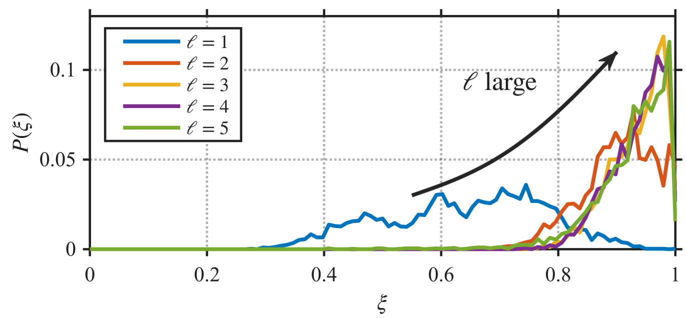


Fig. 2: Distribution $P(\xi)$ of coverage $\xi$ over interval order $\ell$.

$v$ increases. A clear concentration effect is observed: the distribution progressively shifts toward the right endpoint, indicating that a larger fraction of Monte Carlo samples achieve near-complete dimensional coverage under higher interval orders. This rightward probability mass accumulation provides stronger statistical evidence that the constructed intervals more reliably enclose the true OPF solution across all state dimensions.

**2) Impact of uncertainty dimension**

To assess the impact of the uncertainty dimension, Fig. 3 compares Monte Carlo and *IntervalOPF* results as the number of selected uncertain buses increases from $n_{\mathrm{u}} = 2$ to $n_{\mathrm{u}} = 4$. In both settings, the IntervalOPF boxes fully enclose $\theta_1$ and $\theta_2$ on the 2D plane, and the case with $n_{\mathrm{u}} = 4$ produces visibly tighter enclosures due to the larger number of intervals. Consistent with this observation, Table I shows that the coverage percentage increases as $n_{\mathrm{u}}$ grows, indicating that higher uncertainty dimension leads to improved alignment between the constructed intervals and the observed Monte Carlo solution set.

**3) Impact of uncertainty level**

Figure 4 illustrates the impact of different uncertainty levels

979-8-3315-8138-1

on the 39-bus system. We consider three relative load uncertainty ranges: $[0.9, 1.1]$ (10%), $[0.8, 1.2]$ (20%), and $[0.7, 1.3]$ (30%). For each uncertainty level, the IntervalOPF enclosure is plotted together. As the uncertainty range widens, the Monte Carlo solutions exhibit a larger spread and the resulting variable variations increase accordingly. Across all three uncertainty levels, the IntervalOPF box encloses the Monte Carlo results well on the displayed 2D projection, indicating that the method adapts reliably to different magnitudes of load uncertainty and scales appropriately with the resulting variability.

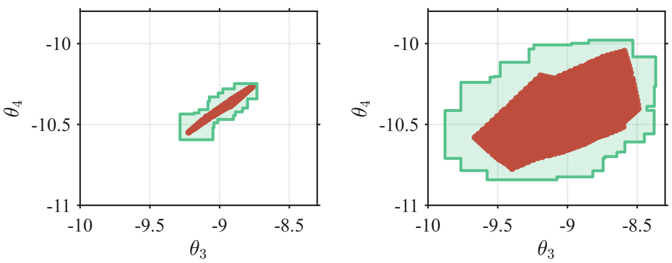


(a) $n_{\mathrm{u}} = 2$ (b) $n_{\mathrm{u}} = 4$

Fig. 3: Impact of uncertainty dimension on IntervalOPF

### C. Scalability Analysis of IntervalOPF

As shown in Table I, the measured runtimes follow the predicted complexity scalings: for a single case, the Monte Carlo cost grows approximately as $d^{n_{\mathrm{u}}}$, whereas the IntervalOPF cost grows as $\ell^{n_{\mathrm{u}}}$. As a result, the empirical speedup factor $(d/\ell)^{n_{\mathrm{u}}}$ demonstrates that the computational advantage of IntervalOPF scales polynomially in the ratio $d/\ell$ and exponentially in $n_{\mathrm{u}}$.

When the system size increases across cases, the computational costs of both Monte Carlo and IntervalOPF rise at comparable rates, indicating that case size affects the two approaches in a similar manner. Because the speedup factor $(d/\ell)^{n_{\mathrm{u}}}$ remains substantial under all tested system sizes, the overall runtime of IntervalOPF stays well within a practical range even as the network grows. This behavior confirms that the proposed method maintains strong scalability, with the speedup compensating for the increased system dimension in a consistent and predictable way.

## V. Conclusion

This work proposed a new interval construction framework for reliably estimating OPF solution enclosure under load uncertainty. The method requires only one additional OPF evaluation within the uncertainty interval and therefore remains lightweight and easy to deploy at scale. We established theoretical foundations for the approach by analyzing the Lipschitz continuity of the OPF solution mapping, which provides justification for the resulting interval estimates. Extensive experiments on standard OPF benchmarks demonstrated that the method produces tight enclosures while achieving substantial computational savings compared with exhaustive Monte Carlo samplings. These results indicate that the proposed approach is both accurate and scalable, enabling efficient uncertainty-aware OPF analysis in high-dimensional systems.

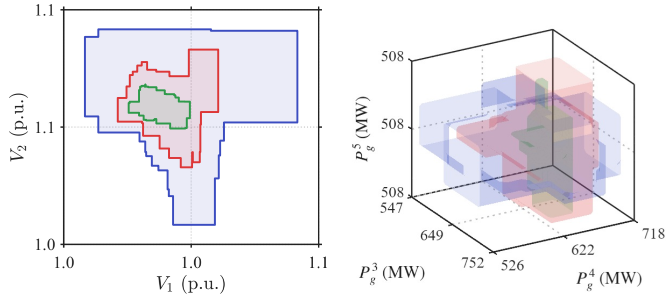


(a) Projection on 2D space (b) Projection on 3D space

Fig. 4: Impact of uncertainty level on IntervalOPF. Periwinkle-30% uncertainty, Red-20% uncertainty, Green-10% uncertainty.


## Acknowledgement

This work was supported in part by the National Science Foundation under Grant Nos. ECCS-2432387.


## References


[1] Y. Zhang, S. Shen, and J. L. Mathieu, "Distributionally robust chance-constrained optimal power flow with uncertain renewables and uncertain reserves provided by loads," *IEEE Transactions on Power Systems*, vol. 32, no. 2, pp. 1378–1388, 2016.

[2] C. G. Petra and I. Aravena, "A surrogate-based asynchronous decomposition technique for realistic security-constrained optimal power flow problems," *Operations Research*, vol. 71, no. 6, pp. 2015–2030, 2023.

[3] D. Bienstock, M. Chertkov, and S. Harnett, "Chance-constrained optimal power flow: Risk-aware network control under uncertainty," *SIAM Review*, vol. 56, no. 3, pp. 461–495, 2014.

[4] P. Zhang and W. Li, "Boundary analysis of distribution reliability and economic assessment," *IEEE Transactions on Power Systems*, vol. 25, no. 2, pp. 714–721, 2010.

[5] P. Zhang, *Microgrids: Theory and Practice*. John Wiley & Sons, 2024.

[6] Y. Zhou and P. Zhang, "Neuro-reachability of networked microgrids," *IEEE Transactions on Power Systems*, vol. 37, no. 1, pp. 142–152, 2021.

[7] Y. Zhou, P. Zhang, and M. Yue, "Reachable dynamics of networked microgrids with large disturbances," *IEEE Transactions on Power Systems*, vol. 36, no. 3, pp. 2416–2427, 2020.

[8] Y. Zhou and P. Zhang, "Reachable power flow: Theory to practice," *IEEE Transactions on Power Systems*, vol. 36, no. 3, pp. 2532–2541, 2020.

[9] ——, "Reachable eigenanalysis," *IEEE Transactions on Power Systems*, vol. 35, no. 6, pp. 4936–4939, 2020.

[10] F. Torelli, A. Vaccaro, and N. Xie, "A novel optimal power flow formulation based on the lyapunov theory," *IEEE Transactions on Power Systems*, vol. 28, no. 4, pp. 4405–4415, 2013.

[11] J. Nocedal and S. J. Wright, *Numerical optimization*. Springer, 2006.

[12] R. D. Zimmerman and H. Wang, *Matpower Interior Point Solver (MIPS) User's Manual*, version 1.5.2 ed., Power Systems Engineering Research Center (PSERC), 2025.

[13] Y. Zhou and P. Zhang, "Reachable power flow," *IEEE Transactions on Power Systems*, vol. 35, no. 4, pp. 3290–3293, 2020.

[14] H. Wang, C. E. Murillo-Sanchez, R. D. Zimmerman, and R. J. Thomas, "On computational issues of market-based optimal power flow," *IEEE Transactions on power Systems*, vol. 22, no. 3, pp. 1185–1193, 2007.

[15] M. Althoff, O. Stursberg, and M. Buss, "Reachability analysis of nonlinear systems with uncertain parameters using conservative linearization," in *2008 47th IEEE Conference on Decision and Control*, 2008.

[16] P.-J. Meyer, A. Devonport, and M. Arcak, *Interval reachability analysis: Bounding trajectories of uncertain systems with boxes for control and verification*. Springer Nature, 2021.

[17] J. Anderson, F. Zhou, and S. H. Low, "Worst-case sensitivity of dc optimal power flow problems," in *2020 American Control Conference (ACC)*, 2020.

[18] G. E. Coxson, "Computing exact bounds on elements of an inverse interval matrix is np-hard," *Reliable Computing*, vol. 5, no. 2, pp. 137–142, 1999.



979-8-3315-8138-1